



Statistical Properties of Alfvén Ion Cyclotron Waves and Kinetic Alfvén Waves in the Inner Heliosphere

Chang Sun^{1,2,3}, Lei Yang^{1,2,3}, Qiu-Huan Li^{4,5}, Cun-Li Dai⁶, Jian-Ping Li⁷, Zheng-Wei Cheng³, and De-Jin Wu^{1,2}

¹Key Laboratory of Planetary Sciences, Purple Mountain Observatory, CAS, Nanjing 210023, China; ylei@pmo.ac.cn

²School of Astronomy and Space Sciences, University of Science and Technology of China, Hefei 230026, China

³State Key Laboratory of Space Weather, National Space Science Center, CAS, Beijing 100190, China

⁴Institute of Space Physics, Luoyang Normal University, Luoyang 471934, China

⁵Henan Key Laboratory of Electromagnetic Transformation and Detection, Luoyang Normal University, Luoyang 471934, China

⁶College of Sciences, Nanjing Agricultural University, Nanjing 210095, China

⁷Key Laboratory of Dark Matter and Space Astronomy, Purple Mountain Observatory, CAS, Nanjing 210023, China

Received 2023 March 31; revised 2023 June 13; accepted 2023 June 14; published 2023 September 6

Abstract

Alfvén ion cyclotron waves (ACWs) and kinetic Alfvén waves (KAWs) are found to exist at <0.3 au observed by Parker Solar Probe in Alfvénic slow solar winds. To examine the statistical properties of the background parameters for ACWs and KAWs and related wave disturbances, both wave events observed by Parker Solar Probe are selected and analyzed. The results show that there are obvious differences in the background and disturbance parameters between ACWs and KAWs. ACW events have a relatively higher occurrence rate but with a total duration slightly shorter than KAW events. The median background magnetic field magnitude and the related background solar wind speed of KAW events are larger than those of ACWs. The distributions of the relative disturbances of the proton velocity, proton temperature, the proton number density, and β cover wider ranges for ACW events than for KAW events. The results may be important for the understanding of the nature and characteristics of Alfvénic slow solar wind fluctuations at ion scales near the Sun, and provide the information of the background field and plasma parameters and the wave disturbances of ACWs and KAWs for further relevant theoretical modeling or numerical simulations.

Key words: (Sun:) solar wind – plasmas – waves – methods: statistical

1. Introduction

The Parker Solar Probe (PSP) (Fox et al. 2016) observations of ion-scale waves have been reported in the near-Sun plasma environment by many studies (e.g., Bowen et al. 2020a; Perrone et al. 2020; Verniero et al. 2020; Klein et al. 2021; Shi et al. 2021; Zhao et al. 2021b; He et al. 2022). The reported ion-scale waves are often Alfvén ion cyclotron waves (ACWs) with wave frequencies around the proton gyrofrequency and kinetic Alfvén waves (KAWs) (Huang et al. 2020; Duan et al. 2021), which will be introduced in more detail below. The KAWs can extend from the ion scales to electron scales, explaining primary turbulence cascade and dissipation at sub-proton scales. The KAWs are also widely believed to be related to turbulent fluctuations at kinetic scales (Liu et al. 2023). The existence of these waves so close to the Sun indicates that these waves may be ubiquitous and associated with small-scale magnetic fluctuations and plasma instabilities in the inner heliosphere. They usually play an important role in the energy dissipation of the solar wind fluctuations and the resultant plasma heating and acceleration.

ACWs are also referred to as ion cyclotron waves and electromagnetic ion cyclotron waves. Quasi-parallel propagating

ACWs have a wavelength around the ion gyroradius and left-handed polarizations in the plasma frame (Jian et al. 2010; He et al. 2011), and are highly linked with the ion temperature anisotropy (Tu et al. 2002; Telloni et al. 2020). In the case of the velocity quasi-aligned with the magnetic field, ACWs occur sporadically in short time intervals (Jian et al. 2009, 2010), and are also found in the fast solar wind (He et al. 2011, 2015; Telloni et al. 2019). At the heliocentric distance of 1 au, ACWs are found to be temporally dependent and their distributions of the wave durations and amplitudes show a power law spectrum (Zhao et al. 2018). PSP is the first mission to in situ measure the solar wind below 0.3 au and observed abundant ACWs during 30%–50% of the encounter intervals in the inner heliospheric solar wind (e.g., Bale et al. 2019; Bowen et al. 2020a, 2020b; Perrone et al. 2020; Verniero et al. 2020; Shi et al. 2021; Zhao et al. 2021b).

Due to the wave frequency being close to the proton gyrofrequency, ACWs can effectively couple with ions through cyclotron resonance and be damped by converting the wave energy to plasma particles. According to the kinetic theory, cyclotron resonance allows for the energization of ions by the perpendicular component of the electric field (Duan et al. 2020;

Klein et al. 2020; Luo et al. 2022). ACWs can also be considered as one evident signature of the resonant dissipation of high-frequency Alfvén waves at frequencies around the gyrofrequency (Telloni et al. 2020), because the ions can be energized by the perpendicular component of the electric field via cyclotron resonance (Duan et al. 2020; Klein et al. 2020; Zhao et al. 2021b; Luo et al. 2022), resulting in strong perpendicular ion heating (Cranmer et al. 1999; Hollweg & Isenberg 2002). Additionally, it is found that ACWs contribute to the wave-particle energy exchange detected by PSP during the third perihelion at 0.23 au (Vech et al. 2021). The ACW characteristics are well accounted for by the Doppler shifted wave frequency, phase speed, and the damping rate, and the wave energy is transmitted to the particles. The dissipation rate spectrum of ACWs is measured in the magnetosheath turbulence (He et al. 2019).

One main generation mechanism for ACWs is anisotropic temperature instabilities through releasing the excess of the ion perpendicular thermal energy, at the same time the wave amplitude reaches a saturation state when the ion thermal anisotropy nears equilibrium. In the solar wind, ACWs can be generated locally (Zhao et al. 2021b; Vech et al. 2021). According to statistical analysis (Telloni et al. 2019), the protons are heated in a direction perpendicular to the magnetic field by the resonant dissipation of high-frequency Alfvén waves, increasing their temperature anisotropy. As a result, the proton velocity distribution exceeds the proton cyclotron instability threshold, which subsequently drives the local formation of ACWs in the solar wind.

More compressible than ACWs, KAWs are another ion-scale wave mode and distinguished by their oblique or quasi-perpendicular propagation and a right-handed polarization (e.g., Gary 1986; Hollweg 1999; Howes 2010; He et al. 2012; Sahraoui et al. 2012; Podesta 2013; Zhao et al. 2016; Huang et al. 2020). Ion-scale or sub-ion-scale solar wind fluctuations are found to contain the properties of KAWs (Leamon et al. 1998; Bale et al. 2005; Sahraoui et al. 2009, 2010; Howes et al. 2011; Podesta 2013; Bruno & Telloni 2015), i.e., quasi-perpendicular propagation angle and right-handed polarizations, and even some good techniques are used, e.g., the k -filtering technique (Sahraoui et al. 2010; Lin et al. 2022), the wave dispersion method (Sahraoui et al. 2009), and the reduced magnetic helicity (Matthaeus & Goldstein 1982; He et al. 2011, 2015).

The kinetic processes associated with KAWs may be important in determining proton temperature in the solar wind (Woodham et al. 2021) and in the observations of steeper perpendicular-wavevector power spectra of magnetic fluctuations below the ion gyroscale (Leamon et al. 1999; Howes et al. 2008a; Schekochihin et al. 2009). The solar wind can be heated by the KAW turbulence via cyclotron/Landau damping or stochastic heating (Parashar et al. 2015; Isenberg & Vasquez 2019; Zhao et al. 2020), mostly results in particle's

parallel heating (e.g., Quataert 1998; Howes et al. 2008a) and ion's perpendicular heating (Isenberg & Vasquez 2019). The parallel heating produced through Landau resonance (Gary & Nishimura 2004; Gary & Borovsky 2008; Howes et al. 2008a) is in agreement with the findings of ion-mass-proportional perpendicular temperatures in fast solar wind (Isenberg & Vasquez 2019). The electromagnetic field energy of the KAWs is shown to strongly dissipate by heating the plasma particles, particularly the electron species in the parallel direction (He et al. 2020). The preferentially perpendicular heating of solar wind protons by KAWs may be the reason for the quick rise in the perpendicular proton temperature and the magnetic helicity magnitude (Zhao et al. 2021a).

Both ACWs and KAWs are found to exist at the heliocentric distance of R within 0.3 au in the slow wind characterized by a high degree Alfvénicity, i.e., a highly correlated velocity and magnetic field fluctuations (also called Alfvénic slow wind) (e.g., Huang et al. 2020; Telloni et al. 2020). The magnetic compressibility level of KAWs is observed to be much higher than ACWs in the Alfvénic slow wind, and the interpretation in terms of ACWs and KAWs is supported by the low (high) magnetic compressibility displayed by parallel (perpendicular) fluctuations at frequencies near the proton gyrofrequency (Telloni et al. 2020), which observationally supports theoretical models predicting that a spectrum of KAWs is the primary source of high-frequency magnetic fluctuations in a low- β solar wind plasma (Howes et al. 2008b; Schekochihin et al. 2009). While the ACWs appear to be constrained by the proton cyclotron kinetic instability threshold and are mostly related to increasing levels of temperature anisotropy, KAWs are found at lower levels of anisotropy and appear to be constrained by the mirror mode instability threshold, extending as well to close to the parallel firehose unstable zone (Telloni et al. 2020). The existence of ACW and KAW is also found in the Alfvénic low speed plasma, which strongly supports the view that the Alfvénic content of solar wind waves at the fluid scales is the key parameter for the generation of driving waves at kinetic scales. In the solar wind turbulence, the resonant dissipation of high-frequency Alfvén waves increases their temperature anisotropy, leading to unstable velocity distribution, which drives the solar wind to produce ACWs locally (Telloni et al. 2019, 2020). Since oblique KAWs preferentially heat the ions in the perpendicular direction, the resulting temperature anisotropy may excite the quasi-parallel-propagating ACWs (Isenberg & Vasquez 2019; Zhao et al. 2021b), which process can be used to explain the existence of both ACWs and KAWs in the Alfvénic slow wind.

Highly Alfvénic slow solar wind flows contain the ion-scale ACWs and KAWs observed by PSP at ~ 0.18 au from the Sun. How do ACWs and KAWs differ from one another in terms of the magnetic and plasma background parameters, and what do both wave disturbances look like in such a plasma environment so close to the Sun? The motivation of the present work is to

examine the statistical properties of the background parameters for ACWs and KAWs and their related wave disturbances in highly Alfvénic slow solar wind. The rest of this paper is organized as follows. Section 2 describes the PSP data and the analysis methods. Case studies of ACWs and KAWs are presented in Section 3. In Section 4, the statistical results of both waves are provided and discussed. The main results and conclusions are summarized in Section 5.

2. Data and Methods

To further investigate ACWs and KAWs in the inner heliosphere, we use the plasma data from the Solar Wind Electron, Alpha, Proton (SWEAP) instrument (Kasper et al. 2016; Case et al. 2020) onboard PSP at sampling frequencies between 1 Sa/cycle and 4 Sa/cycle and the magnetic field data from the FIELDS fluxgate magnetometer (Bale et al. 2016) at the sampling frequency of 256 Sa/cycle (~ 293 Hz) for the Encounter mode, where 1 cycle is about 0.873 s.

The normalized reduced magnetic helicity σ_m is often used to identify the polarization features of solar wind fluctuations (Matthaeus & Goldstein 1982) and of traditional plasma waves (Howes & Quataert 2010; Meyrand & Galtier 2012; Klein et al. 2014). In this study, σ_m is calculated using the same method described in He et al. (2011) to show the presence of ACWs and KAWs presented in the events studied by Huang et al. (2020), in which ion scale fluctuations observed by PSP at 0.18 au are found to contain two populations: ACWs with $\sigma_m > 0$ at 1.4–4.9 Hz (in the spacecraft frame) and $\theta_{BR} > 150^\circ$ and KAWs with $\sigma_m < 0$ at 2.1–26 Hz and $60^\circ < \theta_{BR} < 130^\circ$, and here θ_{BR} is the angle between the local mean magnetic field and the radial direction. Here the PSP data used in this work are reprocessed using bandpass filtering in the KAW and ACW frequency range for all events. The local mean magnetic field is obtained as the mean of the difference between the PSP data and the bandpass filtered data (i.e., the corresponding disturbed quantities). Following the same selection criteria for ACWs and KAWs (Huang et al. 2020), events with frequencies close to the local proton frequency in the spacecraft frame are first selected after visual inspections. ACW and KAW events are classified based on $\theta_{BR} > 150^\circ$ with a positive σ_m and $60^\circ < \theta_{BR} < 130^\circ$ with a negative σ_m , respectively. Then the related event durations and relevant magnetic and plasma parameters are obtained for further analysis. In addition, we simply select events with a duration of more than 1 minute with relatively pure and continuous wave activities for convenient visual inspections and further calculations. Events with duration of less than 1 minute are often intermittent and in a mixed complex state, and will not provide enough data points (≥ 100) for further analysis of the related plasma parameters. Therefore we ignored those events with duration less than 1 minute. The mean values and standard deviations of the relevant parameters are used as the corresponding background parameters and the

related disturbed quantities to show the context and the properties of both wave fluctuations, respectively.

3. Case Studies

A typical ACW event is shown in Figure 1, and is observed by PSP during 2018 November 6 06:36:00 UT and 06:39:42 UT. The region between the red vertical dashed lines indicates the presence of the ACW event with a positive normalized reduced magnetic helicity σ_m (in Figure 1(a)) and an angle quasi-parallel ($\theta_{BR} > 150^\circ$ in Figure 1(i)) to the local mean magnetic field. The frequency range for this ACW event is 1.5–6 Hz. The related magnetic field, proton velocity and the proton number density, radial proton thermal speed, proton temperature, and proton β are also shown in Figure 1. The white solid line in Figure 1(a) represents the local proton cyclotron frequency. The average values of these parameters are: the magnetic field magnitude $|\mathbf{B}| \sim 85.4$ nT, the proton velocity $V_p \sim 298$ km s $^{-1}$, the proton temperature $T_p \sim 31.1$ eV, the proton number density $N_p \sim 305.9$ cm $^{-3}$, and the proton beta $\beta_p \sim 0.54$. It is clear that the magnetic field and the proton velocity are mainly along the radial direction in Figures 1(c) and (d), respectively. Based on the standard deviations, both the magnetic field and velocity have larger perturbations in tangential and normal directions than those in radial direction. For the magnetic field, the disturbances in tangential and normal directions are 14.6 nT and 11.6 nT, respectively, but in the radial direction, the disturbed value is only 2.6 nT. Similarly, for the proton velocity, the tangential and normal disturbances are 16.7 km s $^{-1}$ and 24.7 km s $^{-1}$, respectively, but the radial disturbance is only 8.7 km s $^{-1}$. The disturbances in density and temperature are 50 cm $^{-3}$ and 7.35 eV, respectively.

Figure 2 shows a typical KAW event observed by PSP during 2018 November 6 15:02:25 UT and 15:11:21 UT. The region between the red vertical dashed lines indicates the presence of the KAW event with a negative normalized reduced magnetic helicity σ_m (in Figure 2(a)) and an angle quasi-perpendicular ($80^\circ \leq \theta_{BR} \leq 120^\circ$ in Figure 2(i)) to the local mean magnetic field. The frequency range for this KAW event is 2.2–20 Hz. The related magnetic field, proton velocity and proton number density, radial proton thermal speed, proton temperature, and proton β are also shown in Figure 2. The average values of these parameters are: the magnetic field magnitude $|\mathbf{B}| \sim 91.1$ nT, the proton velocity $V_p \sim 416.8$ km s $^{-1}$, the proton temperature $T_p \sim 54.4$ eV, the proton number density $N_p \sim 277.8$ cm $^{-3}$, and the proton beta $\beta_p \sim 0.74$. It is clear that the magnetic field is mainly along the tangential direction in Figure 2(c), and proton velocity is mainly along the radial direction in Figure 2(d). Based on the standard deviations of the magnetic field in this event, the disturbed normal component is 18.2 nT, and the disturbed radial and tangential components are 9.5 nT and 6.9 nT,

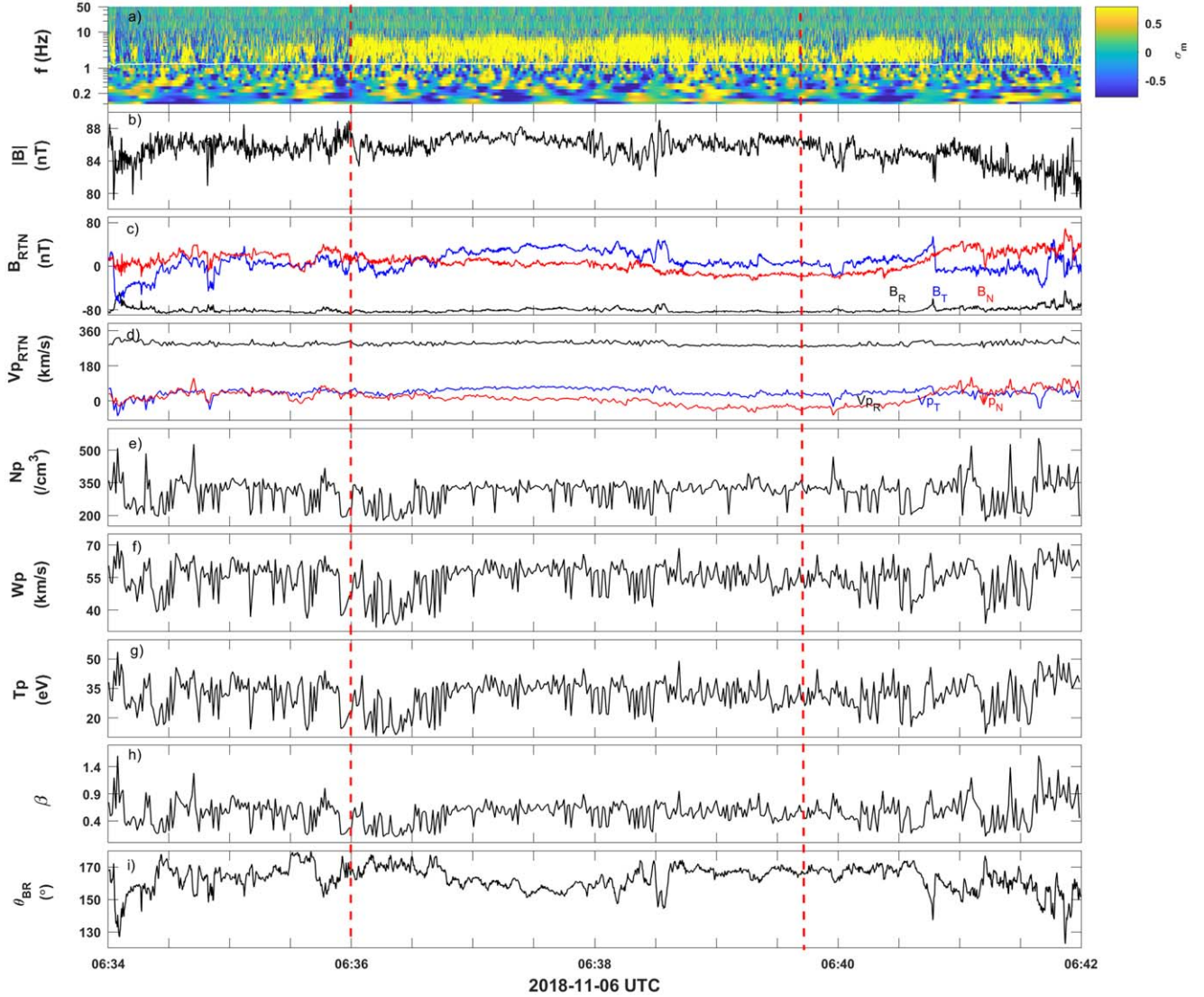


Figure 1. Overview of the magnetic field and plasma data for an ACW event observed by PSP on 2018 November 6: (a) the normalized reduced magnetic helicity σ_m , (b) the magnetic field magnitude $|B|$, (c) the three components of the magnetic field B_R , B_T , B_N , (d) the three components of the proton velocity V_{pR} , V_{pT} , V_{pN} , (e) proton number density N_p , (f) radial proton thermal speed W_p , (g) proton temperature T_p , (h) proton beta β , and (i) the angle θ_{BR} between the radial direction and the local background magnetic field. The region between the red vertical dashed lines indicates the presence of the wave event. The white solid line in (a) represents the local proton cyclotron frequency.

respectively. Similarly, the disturbed velocity is also mainly in the normal direction. The disturbed normal velocity is 14.08 km s^{-1} , much higher than the other two components. The disturbances in density and temperature are 18.67 cm^{-3} and 4.24 eV , respectively.

4. Statistical Results

For statistical analysis, a total of 80 events are identified from PSP observations for the whole day of 2018 November 06, which has been reported by Huang et al. (2020). The total duration of these events is 214.58 minutes (14.9% of the whole day), and it should be noted that the duration of selected ACW and KAW

events is 1 minute or more, and we ignore those events with duration less than 1 minute. Of these events, the longest duration is 11 minutes. There are 33 KAW events (41.25% of the number of all events) with a corresponding total duration of 122 minutes (56.85% of the duration of all wave events) and 47 ACW events (58.75% of the number of all events) with a corresponding total duration of 92.6 minutes (43.15% of the duration of all wave events). These results show that ACW events have a relatively higher occurrence rate but a relatively shorter duration than KAW events in the slow solar wind at 0.18 au from the Sun.

To examine the background magnetic and plasma environments, Figure 3 indicates the distributions of the averages of

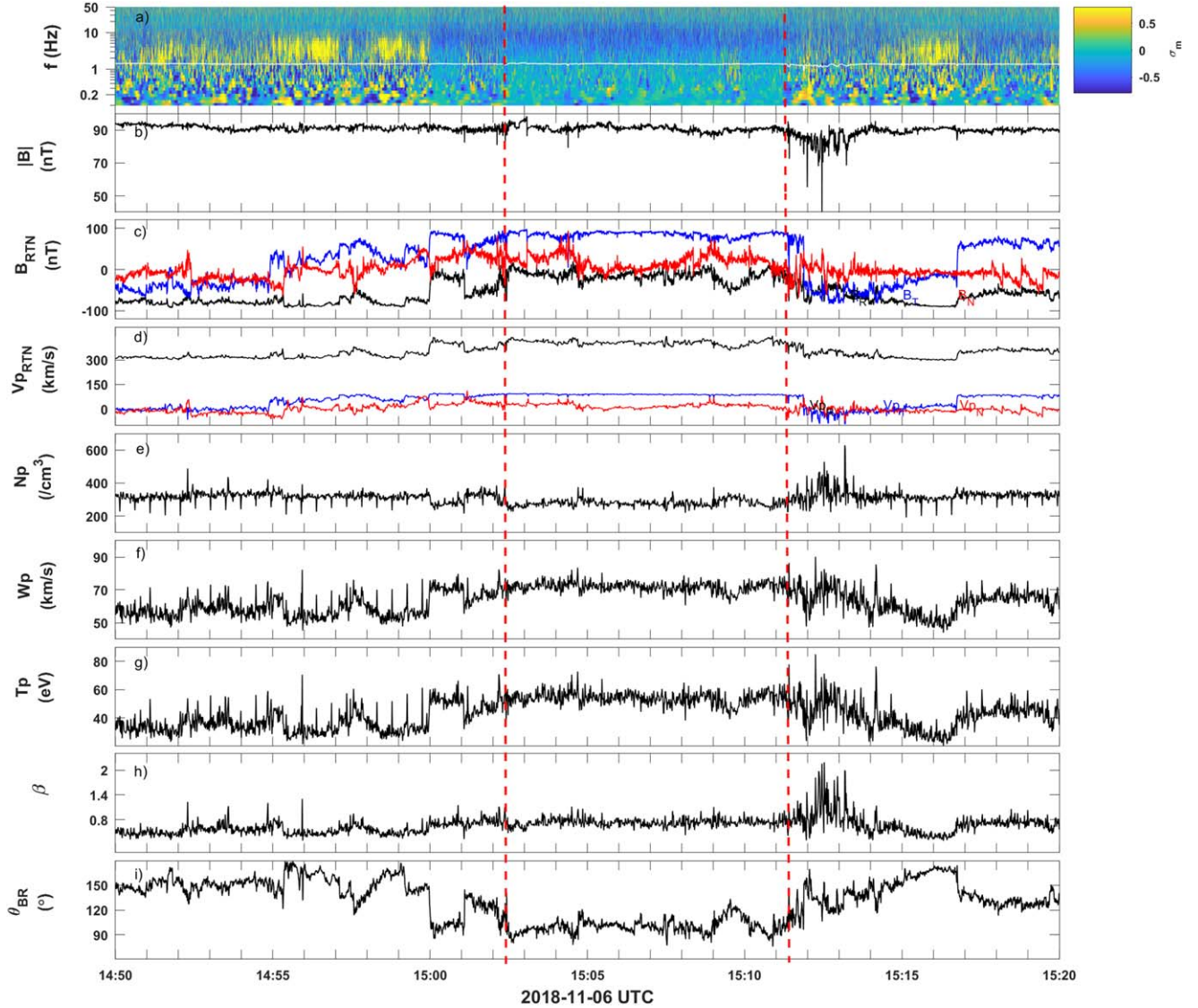


Figure 2. Overview of the magnetic field and plasma data for a KAW event observed by PSP on 2018 November 6. The relevant parameters and format are the same as those of Figure 1.

various parameters of each ACW (red lines) and KAW (blue lines) event observed by PSP. These parameters are the magnetic field magnitude $|\mathbf{B}|$, the magnetic field components B_R , B_T , B_N , the proton velocity magnitude $|\mathbf{V}_p|$, the proton velocity components V_{pR} , V_{pT} , V_{pN} , the wave event duration, the proton temperature T_p , the proton number density N_p , and the proton beta β . The relevant median values of all ACW (KAW) parameters are highlighted by the red (blue) vertical dashed lines in Figure 3.

The median background magnetic field magnitude of KAW (ACW) events is about 94 nT (87 nT) in Figure 3(a) and the related background speed is about 378 km s^{-1} (309 km s^{-1}) in Figure 3(e), which indicates that the background magnetic field

magnitude of most KAW events is stronger than that of ACWs and their related background solar wind speed is faster than that of ACWs. In the RTN coordinate system, along the radial direction R , the median value of the background B_R of KAW events is about -21 nT , and that of ACW events is about -81 nT in Figure 3(b), where the positive (negative) sign represents the antisunward (sunward) radial direction. It can be seen that the median of the background B_R of ACW events is larger than that of KAW events in Figure 3(b), but the median of the background V_{pR} of KAW events is about 1.2 times of that of ACW events in Figure 3(f). In the tangential (T) direction, the median of the background B_T of ACW events is weaker than that of KAW events in Figure 3(c), i.e., only

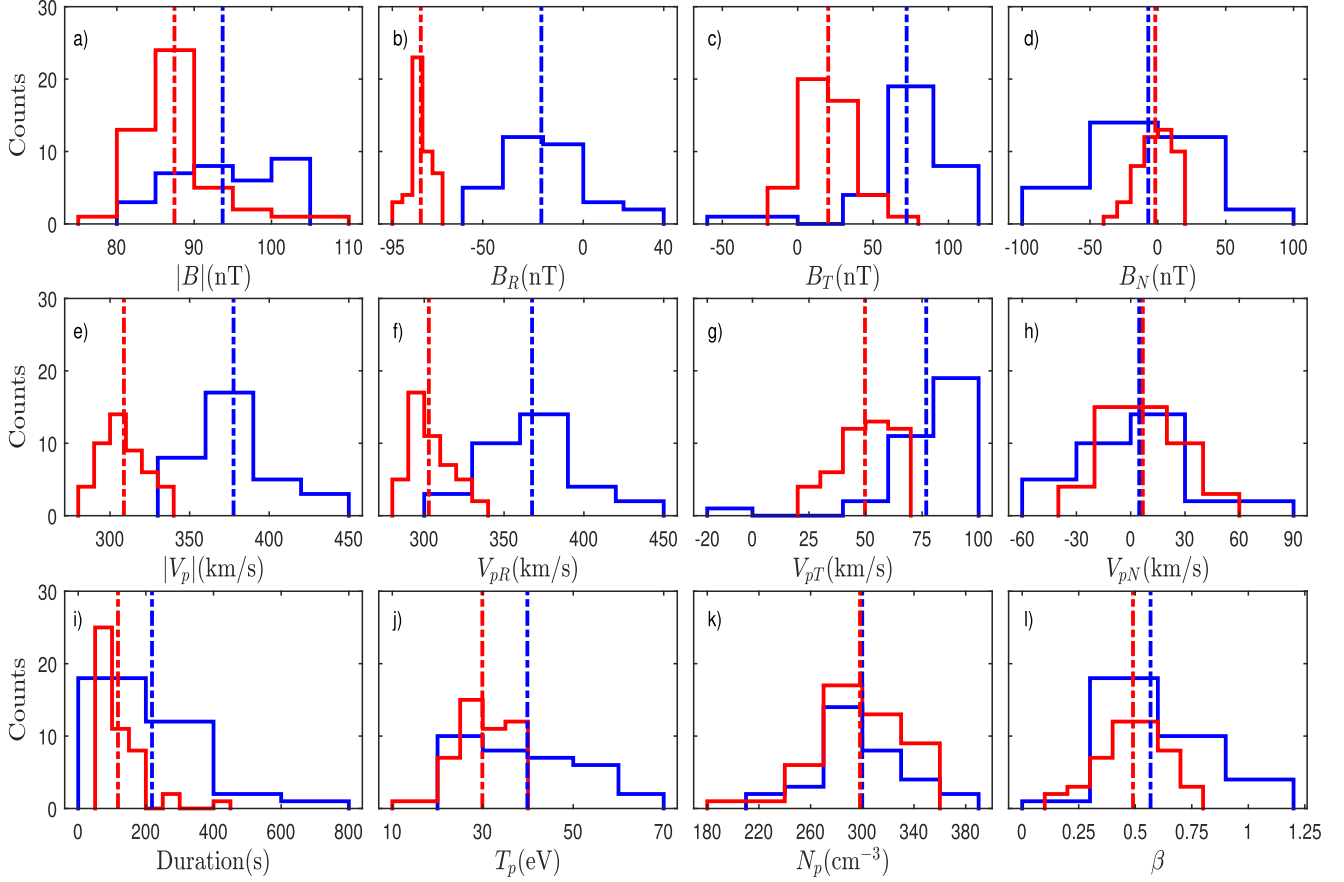


Figure 3. Distributions of (a) the magnetic field magnitude $|\mathbf{B}|$ (b)–(d) the three components of the magnetic field B_R , B_T , B_N , respectively, (e) the proton velocity magnitude $|\mathbf{V}_p|$, (f)–(h) the three components of the proton velocity V_{pR} , V_{pT} , V_{pN} , respectively, (i) the wave event duration, (j) the proton temperature T_p , (k) the proton number density N_p , and (l) the proton beta β for ACW (red lines) and KAW (blue lines) events observed by PSP. The red (blue) vertical dashed lines indicate the median values of relevant ACW (KAW) parameters.

0.28 times that of KAW events, and the median of the background V_{pT} of ACW events is slightly smaller than that of KAW events, i.e., about 65% of that of KAW events in Figure 3(g). In the normal (N) direction, both the medians of the background B_N and the background V_{pN} are similar in Figures 3(d) and (h). In Figure 3(i), the duration of all the wave events ranges from 60 to 660 s, and the median KAW events duration is longer than that of ACW events, but the occurrence rate (or the counts) of ACW events is slightly higher than that of KAW events. The medians of both the background temperature T_p and β of KAW events are higher than those of ACW events in Figures 3(j) and (l), respectively, but the medians of the background proton number density N_p of both wave events are nearly the same in Figure 3(k).

To further study the observational properties of ACW and KAW events in the inner heliosphere, the disturbances of the magnetic field and velocity are calculated from the standard deviations of the corresponding parameters from Figures 3(a)–(h). Figure 4 shows the distribution of these disturbances for the

ACW (red lines) and KAW (blue lines) events. In general, the magnetic field magnitude disturbance $\delta|\mathbf{B}|$ is very small compared with their corresponding magnetic field magnitude $|\mathbf{B}|$ (around 90 nT) in Figure 3(a), i.e., the median values of $\delta|\mathbf{B}|$ for ACW and KAW events are around 0.10 nT and 0.17 nT, respectively, in Figure 4(a). It is obvious that the median $\delta|\mathbf{B}|$ of KAW events is slightly larger than that of ACW events. For the RTN components, all the medians for the disturbed magnetic field components of the wave events are larger than that of $\delta|\mathbf{B}|$ in Figures 4(b) and (d). In the radial direction, the median δB_R of ACW events is about 0.18 nT, smaller than that of KAW events (about 0.36 nT) in Figure 4(b). In the tangential direction, the median δB_T of KAW events is smaller than that of ACW events with a difference of 0.12 nT in Figure 4(c), but in the normal direction, the median δB_N of KAW events is larger than that of ACW events in Figure 4(d). The medians of both the total proton speed disturbance $\delta|\mathbf{V}_p|$ and the disturbance of the radial velocity component δV_{pR} are larger for KAW events than for ACW events in Figures 4(e) and (f), but in the tangential and

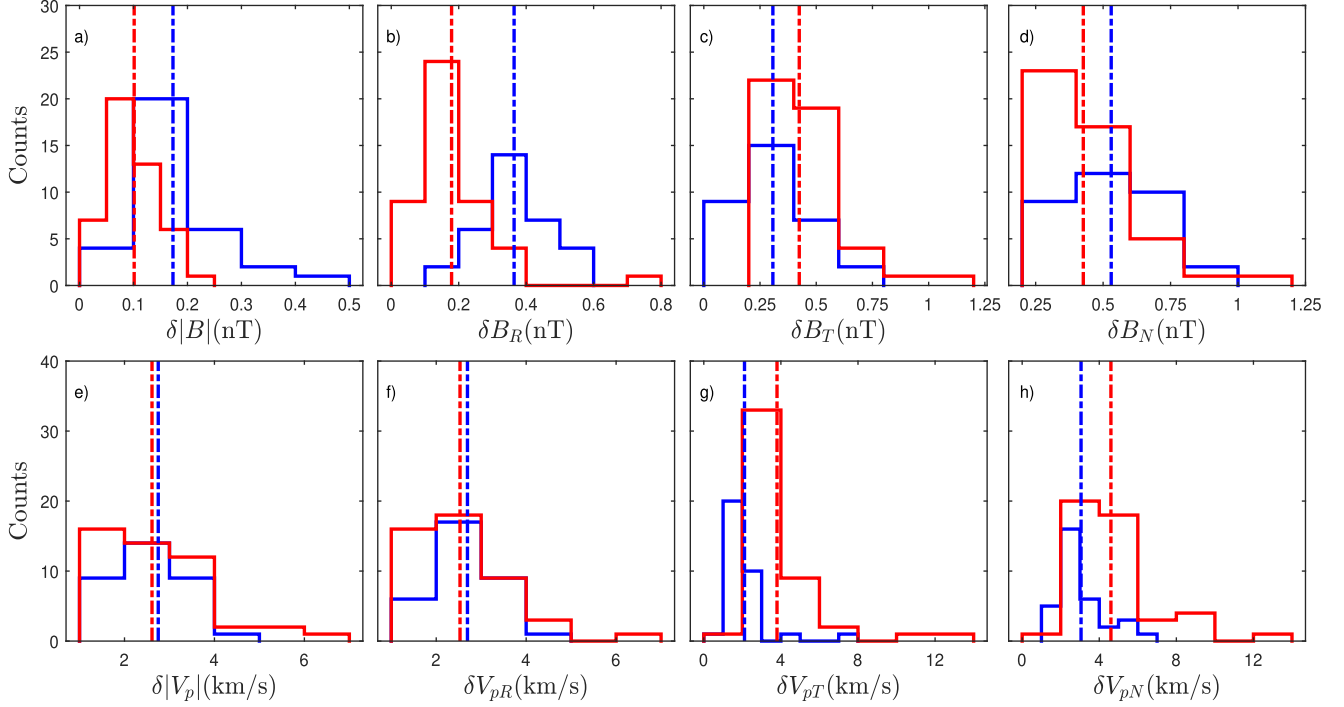


Figure 4. Distributions of the disturbed magnetic field and plasma velocity for ACW (red lines) and KAW (blue lines) events observed by PSP. Here the parameters are the disturbances of the corresponding parameters shown in Figures 3(a)–(h), and the line style is same as that in Figure 3.

normal directions, the median δV_{pT} and median δV_{pN} of KAW events is smaller than those of ACW events in Figures 4(g) and (h).

Besides the magnitudes ($|\delta \mathbf{B}|$ and $|\delta \mathbf{V}_p|$) and the corresponding relative disturbances (with respect to their means, i.e., $|\delta \mathbf{B}|/B$ and $|\delta \mathbf{V}_p|/V_p$) of the magnetic field and the velocity disturbances, Figure 5 displays the disturbances (i.e., δT_p , δN_p , and $\delta \beta$) and the corresponding relative disturbances (i.e., $\delta T_p/T_p$, $\delta N_p/N_p$, and $\delta \beta/\beta$) of the proton temperature, the proton number density, and the proton beta, calculated from the standard deviations of the corresponding parameters from Figures 3(j)–(l), for ACW (red lines) and KAW (blue lines) events. It is obvious that both medians of $|\delta \mathbf{B}|$ and $|\delta \mathbf{B}|/B$ are larger for KAW events than for ACW events in Figures 5(a) and (f), where the median $|\delta \mathbf{B}|$ of ACWs is about 0.87 times that of KAWs and both medians of $|\delta \mathbf{B}|/B$ are around 0.007. The medians of $|\delta \mathbf{V}_p|$, δT_p , δN_p , and $\delta \beta$ and the corresponding relative ones (i.e., $|\delta \mathbf{V}_p|/V_p$, $\delta T_p/T_p$, $\delta N_p/N_p$, and $\delta \beta/\beta$) are larger for ACW events than for KAW events in Figures 5(b)–(e) and (g)–(j).

The median values of $|\delta \mathbf{V}_p|$ for ACW and KAW events are between 4 and 7 km s⁻¹ in Figure 5(b), while the median $|\delta \mathbf{V}_p|/V_p$ of ACW events is about 1.4 times that of KAW events in Figure 5(g). The median values of δT_p for KAW and ACW events are between 2–3 eV in Figure 5(c), and the median $|\delta \mathbf{T}_p|/T_p$ of ACW events is about 1.34 times that of

KAW events in Figure 5(h) where $|\delta \mathbf{T}_p|/T_p$ of ACWs is from 0.052 to 0.286, ~ 5.57 times larger than the distribution width (0.034–0.076) of that of KAWs. Similarly, the median δN_p of ACW (KAW) events is 0.071 (0.036) cm⁻³, and the distribution of ACW events covers a wider range than that of KAW events in Figure 5(d). The distribution of $\delta N_p/N_p$ of ACW events also covers a range (0–0.40) much wider than that of KAW events (0.02–0.07) in Figure 5(i). For KAW events, the related median $\delta \beta$ is only 0.045, but the median $\delta \beta$ of ACW events is 0.061 in Figure 5(e). The distribution of $\delta \beta/\beta$ for ACW events is in the range of 0–0.47, which is much larger than that (0.05–0.12) for KAW events in Figure 5(j). It is clear that the distributions of the relative disturbances of the proton velocity, the proton temperature, the proton number density, and β cover wider ranges for ACW events than for KAW events in Figures 5(g)–(j).

Figure 6 shows the distribution of the θ_{BR} for the ACW (red lines) and KAW (blue lines) events and the θ_{BR} is the angle between the local mean magnetic field and the radial direction. The median values of θ_{BR} for ACW (red vertical dashed line) and KAW events (blue vertical dashed line) are around 163° and 104°, respectively, in Figure 6. It is clear that most ACW/KAW events show quasi-parallel/quasi-perpendicular propagation directions relative to the local mean magnetic field (e.g., Jian et al. 2009, 2010; Verniero et al. 2020; Bowen et al. 2020a). The angle distribution is consistent with the results of

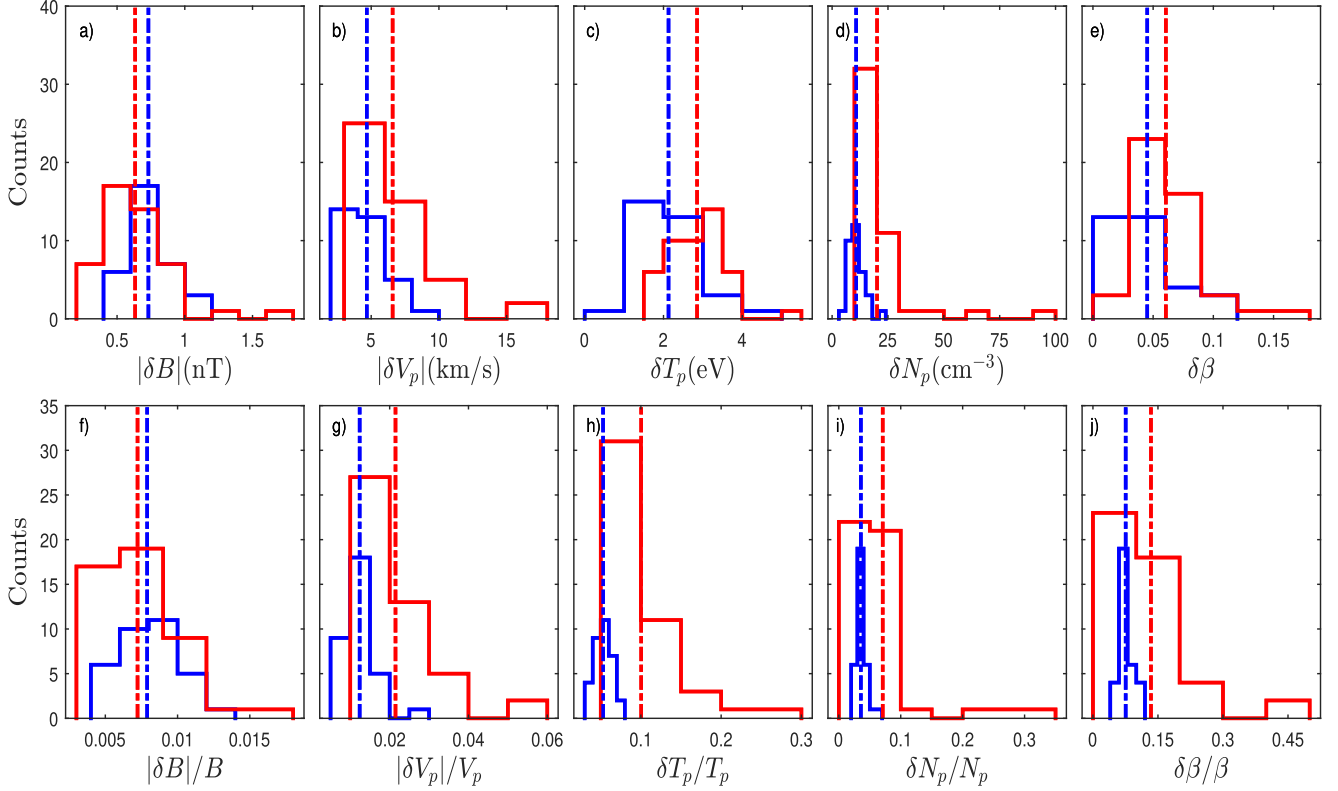


Figure 5. Distributions of (a) the disturbed magnetic field magnitude $|\delta B|$, (b) the disturbed proton velocity magnitude $|\delta V_p|$, (c) the disturbed proton temperature δT_p , (d) the disturbed proton number density N_p , (e) the disturbed proton beta $\delta\beta$, and (f)–(j) the corresponding relative quantities of (a)–(e) with respect to their means, respectively, for ACW (red lines) and KAW (blue lines) events observed by PSP. The red (blue) vertical dashed lines indicate the median values of relevant ACW (KAW) parameters.

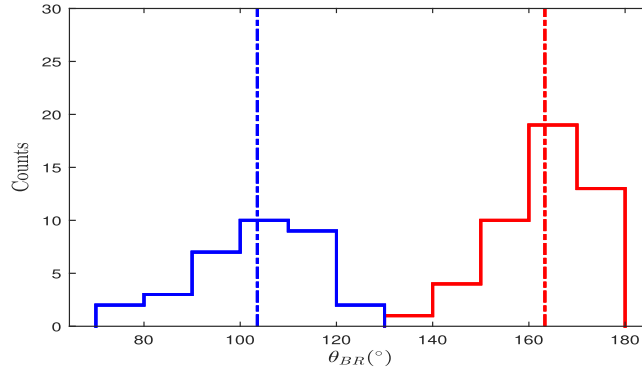


Figure 6. Distributions of the angle θ_{BR} for ACW (red line) and KAW (blue line) events observed by PSP. The red (blue) vertical dashed lines indicate the median values of θ_{BR} for relevant ACW (KAW) events.

Figure 3 (a) by Huang et al. (2020), in which the KAW events are for $60^\circ < \theta_{BR} < 130^\circ$ and the ACW events are for $150^\circ < \theta_{BR} < 180^\circ$. As pointed out by Huang et al. (2020), although the angle varies in time over the range from 60° to 180° , it does not change much in the frequency range ~ 0.1 – 20 Hz and possibly change on larger timescales, i.e., the inertial range or even to the $1/f$ range, which scales are affected by the switchbacks (Dudok de Wit et al. 2020). So the features of and the high frequency of both ACW and KAW events in this work

may exclude the possible effects of the switchbacks. The distributions of the angle cover wider ranges for ACW events than for KAW events in Figure 6.

Figure 7 shows the proton beta β versus the proton temperature T_p for all selected ACW and KAW events, where the red and blue dots indicate ACW and KAW events, respectively, and the red (blue) solid line is the linear fit for ACW (KAW) events. The red (blue) cross on each point in Figure 7 represents the related error bar of one sigma range for

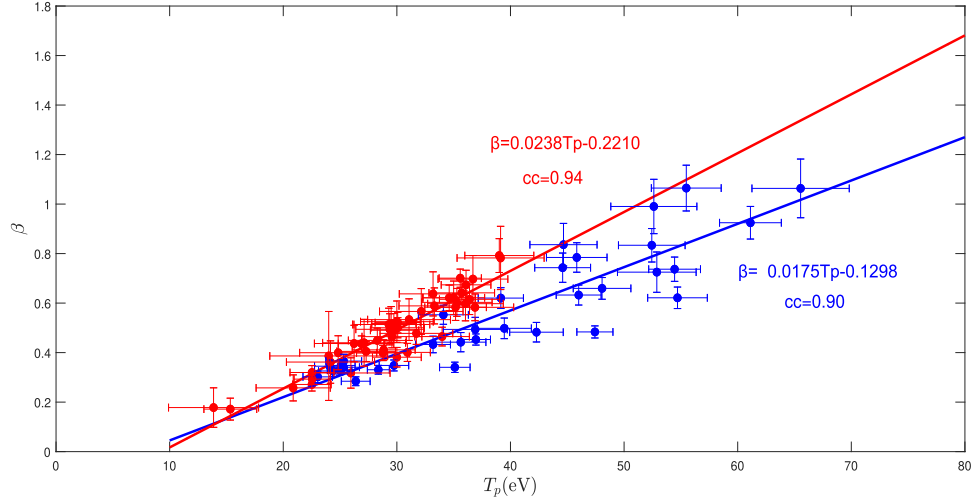


Figure 7. Scatter plots of the proton beta β against the proton temperature T_p for ACWs (red) and KAWs (blue). The red and blue solid lines show the linear fit for the data of ACW and KAW events, respectively, and cc is the relevant correlation coefficient between β and T_p .

each ACW (KAW) event. It is obvious that the red dots of ACW events are closer to its fitted line than the blue dots of KAW events are. For ACW events, β is mainly in 0–0.8, T_p is mainly between 10 eV and 40 eV, and for KAW events, β is mainly in 0.2–1.2, T_p is mainly between 20 eV and 70 eV. The slope of the fitted curve for KAW events is 0.017, smaller than that (0.023) for ACW events. The correlation coefficient cc between β and T_p of KAW events is 0.90, and that of ACW events is 0.94, which indicates that β and T_p of both waves are highly correlated with a different fitted slope. The well linearly correlated β and T_p with different slopes for both waves are possibly due to the nearly constant magnetic field magnitude and the similar distributions (nearly the same median) of the proton number density N_p for ACW and KAW events in Figure 3(k) but with different distributions (different medians) of the proton temperature T_p for both waves in Figure 3(j). The distributions of KAW and ACW events are different in the β - T_p plane of Figure 7.

5. Summary and Conclusions

The ion-scale ACWs and KAWs have been found to be present in highly Alfvénic slow solar wind flows observed by PSP at about 0.18 au from the Sun. What are the characteristics of ACWs and KAWs with respect to the background magnetic and plasma parameters, and what are the features of both wave disturbances in such an environment so close to the Sun? In order to find solutions to both questions, we utilize the magnetic and plasma data obtained from the PSP mission, including the SWEAP (at sampling frequencies between 1 Sa/cycle and 4 Sa/cycle) and FIELDS fluxgate magnetometer measurements (at a sampling frequency of 256 Sa/cycle) to investigate the statistical properties of ACWs and KAWs and

their related wave disturbances in the highly Alfvénic slow solar wind. In the present work, we select 80 individual ACW and KAW wave events, reported by Huang et al. (2020), based on the NASA’s PSP observations of a slow solar wind in the inner heliosphere on 2018 November 6 for further statistical analyses. Our statistical results show that the distributions for the related parameters of both wave events are obviously different, which are summarized as follows.

1. There are 47 ACWs events (58.75% of the counts of all wave events) with a corresponding duration of 92.6 minutes (43.15% of the total duration of all wave events) and 33 KAWs events (41.25% of the counts of all wave events) with a corresponding duration of 122 minutes (56.85% of the total duration of all wave events). The longest wave duration is 11 minutes. ACW events exhibit a relatively higher occurrence rate but with a total duration slightly shorter than KAW events during the slow solar wind interval at 0.18 au from the Sun.
2. For the background magnetic and plasma environments, the median background magnetic field magnitude $|\mathbf{B}|$ and the related background solar wind speed $|V_p|$ of KAW events are larger than those of ACWs. In the RTN coordinates, the medians of the background B_T , V_{pR} , V_{pT} , T_p and β of KAW events are larger than those of ACW events, but the median of the background B_R of ACW events is larger than that of KAW events. The medians of the background B_N , V_{pN} , and proton number density N_p are nearly the same for both wave events.
3. For both wave disturbances, in general, the magnetic field magnitude disturbance $\delta|\mathbf{B}|$ is very small compared with their corresponding magnetic field magnitude $|\mathbf{B}|$, and the median $\delta|\mathbf{B}|$ of KAW events is slightly larger than that of

ACW events. For the RTN components, the medians of the disturbances $|\delta B|$, $|\delta B|/B$, δB_R , δB_N , $\delta|V_p|$, and δV_{pR} for ACW events are smaller than those for KAW events, but for KAW events, the medians of δB_T , $|\delta V_p|$, δV_{pT} , δV_{pN} , δT_p , δN_p , $\delta\beta$, and of the relative disturbances $|\delta V_p|/V_p$, $\delta T_p/T_p$, $\delta N_p/N_p$, and $\delta\beta/\beta$ are smaller than those of ACW events. The distributions of the relative disturbances of the proton velocity, the proton temperature, the proton number density, and β cover wider ranges for ACW events than for KAW events.

- In the β - T_p plane, the distributions of KAW and ACW events have different fitted slopes, and the slope of KAW events is smaller than that of ACW events. The ACW events are more closer to its fitted line than KAW events are. The cause of highly correlated β with T_p for both waves may be the nearly constant magnetic field magnitude and the similar distributions (almost the same median) of N_p for KAW and ACW events but with different distributions (different medians) of T_p for both waves.

The above statistical properties of ACWs and KAWs in the inner heliosphere may be important for the understanding of the nature and characteristics of highly Alfvénic slow solar wind fluctuations at ion scales near the Sun, and provide the information of the background field and plasma parameters and the wave disturbances of ACWs and KAWs for further relevant theoretical modeling or numerical simulations. Our results in the present study may be not ubiquitous for the inner solar wind context, so more similar events are needed for further analyses to obtain more general and meaningful results on ACWs and KAWs when PSP becomes closer to the Sun. Also, theoretical efforts are also required to carry out to know if and how ACWs can interact with KAWs, which is of vital importance for studies on the related ion cyclotron resonance and relevant plasma instabilities therein.

Acknowledgments

We acknowledge the NASA Parker Solar Probe FIELDS team led by S. D. Bale and the SWEAP team led by J. Kasper for use of data. This work was supported in part by the National Natural Science Foundation of China (NSFC, grant Nos. 41874201, 12250014, 11790302, 42174195, and 11873018) and the Specialized Research Fund for State Key Laboratories.

References

Bale, S. D., Badman, S. T., Bonnell, J. W., et al. 2019, *Nat*, **576**, 237
 Bale, S. D., Goetz, K., Harvey, P. R., et al. 2016, *SSRv*, **204**, 49
 Bale, S. D., Kellogg, P. J., Mozer, F. S., Horbury, T. S., & Reme, H. 2005, *PhRvL*, **94**, 215002
 Bowen, T. A., Bale, S. D., Bonnell, J. W., et al. 2020b, *ApJ*, **899**, 74
 Bowen, T. A., Mallet, A., Huang, J., et al. 2020a, *ApJS*, **246**, 66

Bruno, R., & Telloni, D. 2015, *ApJL*, **811**, L17
 Case, A. W., Kasper, J. C., Stevens, M. L., et al. 2020, *ApJS*, **246**, 43
 Cranmer, S. R., Field, G. B., & Kohl, J. L. 1999, *ApJ*, **518**, 937
 Duan, D., He, J., Bowen, T. A., et al. 2021, *ApJL*, **915**, L8
 Duan, D., He, J., Wu, H., & Verscharen, D. 2020, *ApJ*, **896**, 47
 Dudok de Wit, T., Krasnoselskikh, V. V., Bale, S. D., et al. 2020, *ApJS*, **246**, 39
 Fox, N. J., Velli, M. C., Bale, S. D., et al. 2016, *SSRv*, **204**, 7
 Gary, S. P. 1986, *JPIPh*, **35**, 431
 Gary, S. P., & Borovsky, J. E. 2008, *JGRA*, **113**, A12104
 Gary, S. P., & Nishimura, K. 2004, *JGRA*, **109**, A02109
 He, J., Duan, D., Wang, T., et al. 2019, *ApJ*, **880**, 121
 He, J., Marsch, E., Tu, C., Yao, S., & Tian, H. 2011, *ApJ*, **731**, 85
 He, J., Tu, C., Marsch, E., & Yao, S. 2012, *ApJL*, **745**, L8
 He, J., Wang, L., Tu, C., Marsch, E., & Zong, Q. 2015, *ApJL*, **800**, L31
 He, J., Wang, Y., Zhu, X., et al. 2022, *ApJ*, **933**, 220
 He, J., Zhu, X., Verscharen, D., et al. 2020, *ApJ*, **898**, 43
 Hollweg, J. V. 1999, *JGR*, **104**, 14811
 Hollweg, J. V., & Isenberg, P. A. 2002, *JGRA*, **107**, 1147
 Howes, G. G. 2010, *MNRAS*, **409**, L104
 Howes, G. G., Cowley, S. C., Dorland, W., et al. 2008a, *JGRA*, **113**, A05103
 Howes, G. G., Dorland, W., Cowley, S. C., et al. 2008b, *PhRvL*, **100**, 065004
 Howes, G. G., & Quataert, E. 2010, *ApJL*, **709**, L49
 Howes, G. G., Tenborge, J. M., Dorland, W., et al. 2011, *PhRvL*, **107**, 035004
 Huang, S. Y., Zhang, J., Sahrquai, F., et al. 2020, *ApJL*, **897**, L3
 Isenberg, P. A., & Vasquez, B. J. 2019, *ApJ*, **887**, 63
 Jian, L. K., Russell, C. T., Luhmann, J. G., et al. 2009, *ApJL*, **701**, L105
 Jian, L. K., Russell, C. T., Luhmann, J. G., et al. 2010, *JGRA*, **115**, A12115
 Kasper, J. C., Abiad, R., Austin, G., et al. 2016, *SSRv*, **204**, 131
 Klein, K. G., Howes, G. G., TenBerge, J. M., & Podesta, J. J. 2014, *ApJ*, **785**, 138
 Klein, K. G., Howes, G. G., TenBerge, J. M., & Valentini, F. 2020, *JPIPh*, **86**, 905860402
 Klein, K. G., Verniero, J. L., Alterman, B., et al. 2021, *ApJ*, **909**, 7
 Leamon, R. J., Smith, C. W., Ness, N. F., Matthaeus, W. H., & Wong, H. K. 1998, *JGR*, **103**, 4775
 Leamon, R. J., Smith, C. W., Ness, N. F., & Wong, H. K. 1999, *JGR*, **104**, 22331
 Lin, R., He, J., Zhu, X., et al. 2022, *ApJ*, **939**, 121
 Liu, Z. Y., Zong, Q. G., Rankin, R., et al. 2023, *Nat*, **14**, 2088
 Luo, Q., Zhu, X., He, J., et al. 2022, *ApJ*, **928**, 36
 Matthaeus, W. H., & Goldstein, M. L. 1982, *JGR*, **87**, 6011
 Meyrand, R., & Galtier, S. 2012, *PhRvL*, **109**, 194501
 Parashar, T. N., Salem, C., Wicks, R. T., et al. 2015, *JPIPh*, **81**, 905810513
 Perrone, D., Bruno, R., D'Amicis, R., et al. 2020, *ApJ*, **905**, 142
 Podesta, J. J. 2013, *SoPh*, **286**, 529
 Quataert, E. 1998, *ApJ*, **500**, 978
 Sahrquai, F., Belmont, G., & Goldstein, M. L. 2012, *ApJ*, **748**, 100
 Sahrquai, F., Goldstein, M. L., Belmont, G., Canu, P., & Rezeau, L. 2010, *PhRvL*, **105**, 131101
 Sahrquai, F., Goldstein, M. L., Robert, P., & Khotyaintsev, Y. V. 2009, *PhRvL*, **102**, 231102
 Schekochihin, A. A., Cowley, S. C., Dorland, W., et al. 2009, *ApJS*, **182**, 310
 Shi, C., Zhao, J., Huang, J., et al. 2021, *ApJL*, **908**, L19
 Telloni, D., Bruno, R., D'Amicis, R., et al. 2020, *ApJ*, **897**, 167
 Telloni, D., Carbone, F., Bruno, R., et al. 2019, *ApJL*, **885**, L5
 Tu, C. Y., Wang, L. H., & Marsch, E. 2002, *JGRA*, **107**, 1291
 Vech, D., Martinović, M. M., Klein, K. G., et al. 2021, *A&A*, **650**, A10
 Verniero, J. L., Larson, D. E., Livi, R., et al. 2020, *ApJS*, **248**, 5
 Woodham, L. D., Wicks, R. T., Verscharen, D., TenBerge, J. M., & Howes, G. G. 2021, *ApJ*, **912**, 101
 Zhao, G. Q., Feng, H. Q., Wu, D. J., et al. 2018, *JGRA*, **123**, 1715
 Zhao, G. Q., Lin, Y., Wang, X. Y., et al. 2020, *GeoRL*, **47**, e89720
 Zhao, G. Q., Lin, Y., Wang, X. Y., et al. 2021a, *ApJ*, **906**, 123
 Zhao, J. S., Voitenko, Y. M., Wu, D. J., & Yu, M. Y. 2016, *JGRA*, **121**, 5
 Zhao, L. L., Zank, G. P., He, J. S., et al. 2021b, *ApJ*, **922**, 188